Appl. Phys. B 35, 179–193 (1984)

Applied Physics B Photophysics and Laser Chemistry

Excitation, Inversion, and Relaxation Mechanisms of the HCN FIR Discharge Laser*

David D. Skatrud and Frank C. De Lucia

Department of Physics, Duke University, Durham, NC 27706, USA

Received 21 May 1984/Accepted 30 July 1984

Abstract. Millimeter/submillimeter rotational absorption spectroscopy has been used as a diagnostic probe of a cw HCN discharge laser. This sensitive technique allowed in situ absolute population measurements of a number of vibrational states of HCN (including the upper lasing state) and other pertinent molecules. This unique set of data, which was obtained under a variety of discharge and laser conditions, is directly related to excitation, inversion, and relaxation processes. Along with elucidating several fundamental aspects of inversion and relaxation these results also strongly indicate that the primary laser excitation mechanism is near-resonant energy transfer from vibrationally excited nitrogen, $N_2(v=1)$, to the fundamental symmetric stretching mode of hydrogen cyanide, HCN(100), and subsequent thermal population exchange between HCN (100) and the upper laser state, HCN (110).

PACS: 42.55H, 34.50E, 35.80

The complexity of the HCN laser discharge system, which was empirically discovered in 1964 by Gebbie et al. [1], is reflected in the three years of vigorous debate that ensued before the lasing molecular species and transitions were correctly identified. This assignment, in which the stimulated emission is attributed to a mechanism based on a Coriolis perturbation between vibrational/rotational levels of HCN, was proposed by Lide and Maki [2]. It was strongly substantiated by earlier absolute frequency measurements of Hocker et al. [3] and was unambiguously confirmed by additional measurements subsequently made by Hocker and Javan [4].

The HCN laser system has been studied very extensively (see [5–7] for comprehensive reviews). Data for these studies have been collected by a wide range of techniques: measurement of the laser power as a function of gas mixture, pressure, flow rate, tube temperature, current, Q-switch frequency, discharge length, and cavity parameters; mode studies; chemical pumping; resonator interferometry; mass spectroscopy; and electron and neutral gas temperature measurements. These works contain a great wealth of information that is very useful in elucidating many physical properties of the laser system. However, discharge plasmas are inherently very complex phenomena. The numerous constituents of a glow discharge (free electrons, atoms, ions, radicals, and stable molecules) have a labyrinth of chemical and collisional pathways through which they interact. Consequently, theories of excitation and inversion mechanisms have remained largely a matter of conjecture.

Rotational absorption spectroscopy in the millimeter and submillimeter region provides a sensitive means for measuring absolute concentrations of molecules in specific vibrational states. We have monitored the populations of more than a dozen different vibrational states of HCN (including the upper laser state), the ground vibrational state of CN(X), and the first two vibrational states of CO (which was included as an admixture to our standard gas mix for some investigations).

The vibrational state populations within each of the three bending stacks built upon HCN(000), HCN(100), and HCN(001) were found to be essentially in thermal equilibrium. Although the higher bending modes deviated significantly from thermal equilibrium due to vibrationally excited HCN cascading down the bending stack, these excess populations were much less than those of the stretching modes. This provides a

* Work supported by ARO Contract DAAG-29-83-K-0078

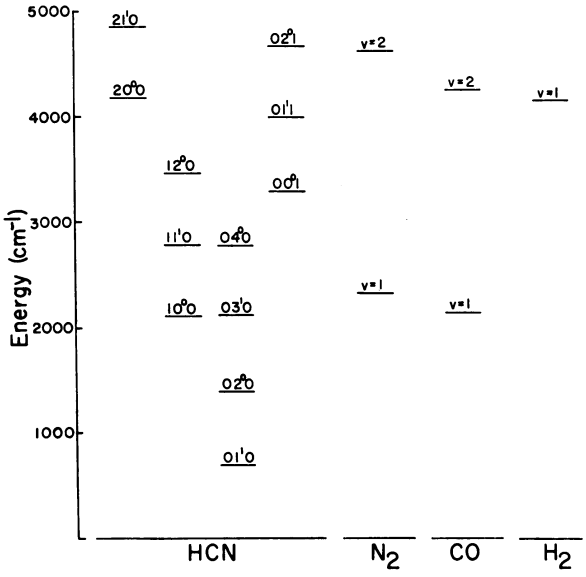

Fig. 1. Vibrational energy levels of HCN, N_2, H_2, and CO

significant reduction in the number of degrees of freedom necessary to describe the vibrational state population distribution of discharge excited HCN and also has several important implications. The rapid exchange of population between adjacent bending states that is required to maintain this equilibrium indicates that a laser induced competition effect in HCN(100) might be expected. This was directly verified by comparison of the lasing and non-lasing populations of HCN(100). The rapid bending exchange also suggests that the requisite tight coupling between HCN(000) and HCN(010) would prevent bottlenecks in this bending stack and this too was experimentally verified. In addition, the bending stack equilibrium provides a simple and quantitative explanation of the dependence of the laser output power on the discharge wall temperature.

The population of HCN(000) peaked around 250 mA with a partial pressure of 7.1 mTorr out of a total pressure of 230 mTorr. The populations of HCN(100) and HCN(001), which were nearly equal, peaked around 500 mA and were greatly in excess of their thermal values. This extreme excitation of HCN(100) and the rapid rate of collisional exchange of one unit of bend for rotational/translational energy (which thermally equilibrates HCN(110) with HCN(100) and also promotes rapid relaxation of HCN(040) down its bending stack) results in a large inversion for the lasing transition. The consistency of these measurements was demonstrated by a calculation of the laser threshold current and excellent agreement with the measured current was found.

The concentration of the CN radical, which is involved in some proposed excitation mechanisms [5, 6], was several orders of magnitude too small to account for the HCN(110) population and laser power. However, the large concentration of vibrationally excited N_2 that exists in low pressure discharges is consistent with the population of HCN(100) and rapid near resonant vibrational transfer via $HCN(000)+N_2(v=1) \rightarrow HCN(100)+N_2(v=0)$. An admixture of CO to our standard gas mixture of CH_4 and N_2 allowed a more quantitative investigation of this mechanism since the vibrational states of CO would be expected to be nearly in equilibrium with those of N_2 (CO, unlike N_2, is amenable to our diagnostic technique since it possesses a permanent electric dipole moment). $CO(v=1)$ was found to be in equilibrium with HCN(100), indicating a direct and rapid exchange between $N_2(v=1)$, $CO(v=1)$, and HCN(100). Furthermore, the changes in the populations of HCN(100) and HCN(001) upon the inclusion of CO in the gas mixture are readily accounted for by near-resonant vibrational transfer and the relative energy defects of CO and N_2 for these processes. These observations, along with other considerations discussed in this paper, show that the primary excitation mechanism in cw HCN discharge lasers is most probably near-resonant vibrational exchange between $N_2(v=1)$ and HCN(100) with the population of the upper lasing state, HCN(110), obtained from HCN(100) by the rapid bending stack thermal equilibration. Although the parameters and mechanisms of other (e.g., pulsed or photolysis driven) HCN lasers may differ, we believe much of what is discussed in this paper is generally applicable.

1. Rotational/Vibrational Energy Levels of HCN

As a linear molecule HCN has three fundamental modes of vibration. The pertinent vibrational states (as well as those for N_2, CO, and H_2) are shown in Fig. 1. In this labeling scheme the first quantum number denotes the symmetric stretch, the second the bending motion, the third the asymmetric stretch, and the superscript is the *l*-type doubling quantum number. The primary lasing transitions are between 11^10 and 04^00. Figure 2 shows the rotational structure of these vibrational states.

In the optical and infrared region, the upper lasing state is often selectively pumped by collisional transfer. This is not a viable means of directly obtaining an inversion in the far infrared since the widths of the collisional transfer resonances, being of the order of kT, are larger than the state separation. HCN circumvents this fundamental limitation by means of a perturbation

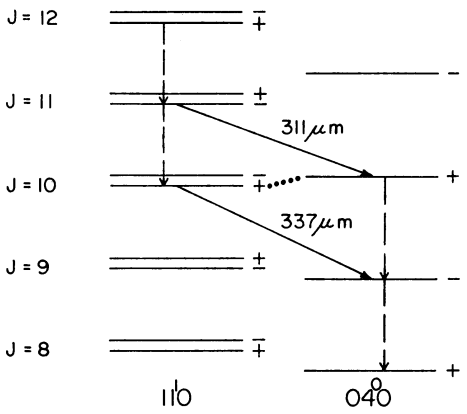

Fig. 2. HCN lasing transitions due to the Coriolis perturbation between the $J=10$ rotational levels of the $11^{1c}0$ and $04^{0}0$ vibrational states. The l-type doubling splitting of the $11^{1}0$ levels is greatly exaggerated. The dashed transitions are less intense emission lines resulting from rotational competition effects

mixing. The ground rotational state of $04^{0}0$ is $2.62\,\mathrm{cm}^{-1}$ below the ground rotational state of $11^{1}0$, however the rotational constant of $04^{0}0$ is larger than that of $11^{1}0$ [8]. As the levels cross at $J=10$, a strong Coriolis perturbation results which effectively mixes these states. Consequently the normally small vibrational transition moment becomes comparable to large pure rotational moments. The population of $11^{1}0$ is greatly in excess of $04^{0}0$ in glow discharges so lasing then occurs on the indicated lines. The less intense intermode lines are due to competition effects between the rotational levels.

2. Rotation Absorption Spectroscopy as a Diagnostic Probe

Millimeter/submillimeter rotational absorption spectroscopy possesses a number of attributes that make it particularly well suited for use as a diagnostic probe of low-pressure glow discharges [9]. The sensitivity at these higher frequencies is much greater than is available at standard microwave frequencies because of the increase in absorption coefficients ($\sim\nu^3$) and decrease in plasma noise ($\sim\nu^2$). This gain must be balanced against decreasing source power. For HCN and our diagnostic system we found the $J=3\leftarrow 2$ transitions around 265 GHz to be favorable. The quasi-optical propagation of the radiation at these shorter wavelengths also provides "remote" sampling without the encumbrances of waveguide. Complimenting the sensitivity is a wide dynamic range: partial pressures varying by more than 10^6 were measured in this study.

The relationship between experimental observables and vibrational state number densities is well defined and contains no terms that introduce fundamental inaccuracies or uncertainties. The vibrational state number density for a diatomic or linear triatomic molecule is given by [10]

$$n=(6.57\times 10^{27})\frac{T^2\Delta\nu}{\mu^2\nu^3 L}\frac{[(J+1)^2]}{[(J+1)^2-l^2]}\left(\frac{\Delta P}{P}\right)\mathrm{cm}^{-3}, \quad (1)$$

where T denotes the kinetic/rotational temperature [K], $\Delta\nu$ the HWHM linewidth of the absorption line [MHz], μ the electric dipole moment of the molecule [D], ν the rotational transition frequency [MHz], L the absorption pathlength [cm], $\Delta P/P$ the fraction of power absorbed, J the rotational quantum number, and l the l-type doubling quantum number (0 for a diatomic).

This relationship is derived with the assumption that $\Delta P/P\ll 1$ so that $\Delta P/P=1-\exp(-\alpha L)\cong\alpha L$, where α is the peak rotational absorption coefficient. This criterion was easily met by either decreasing the pathlength or, in extreme cases, using isotopic species with a small natural abundance. An additional assumption is that the ratio of the populations of the two states involved in the rotational transition is given by the Boltzmann relation with an effective rotational temperature that is equal to the kinetic temperature of the gas. A sensitive check for rotational non-equilibrium was made in a similar pulsed discharge system [9] and no departure from equilibrium was found. This was not a surprising result since rotational relaxation rates are typically gas kinetic ($\sim 10^{-7}$ s at our pressure of ~ 200 mTorr) and consequently lead to rapid rotational equilibrium.

The parameters in (1), with the exceptions of μ and T, are directly measured with our experimental technique. The electric dipole moment μ can be accurately derived from Stark effect measurements and has been tabulated for all molecules of interest in this study. The kinetic/rotational temperature has been measured via thermometry methods by other researchers. An alternate method for determining the temperature, which is employed in this paper, is discussed later.

In practice, the uncertainty in deriving absolute number densities from (1) was limited by the accuracy with which the fraction of absorbed power could be determined. Since our millimeter/submillimeter power was generated by harmonic multiplication and only the lower harmonics were removed by waveguide cutoff sections, part of the power existed in harmonics that were greater than the absorption frequency. This resulted in an uncertainty of approximately 25% in the derived number densities. It should be emphasized that there were several types of measurements that had

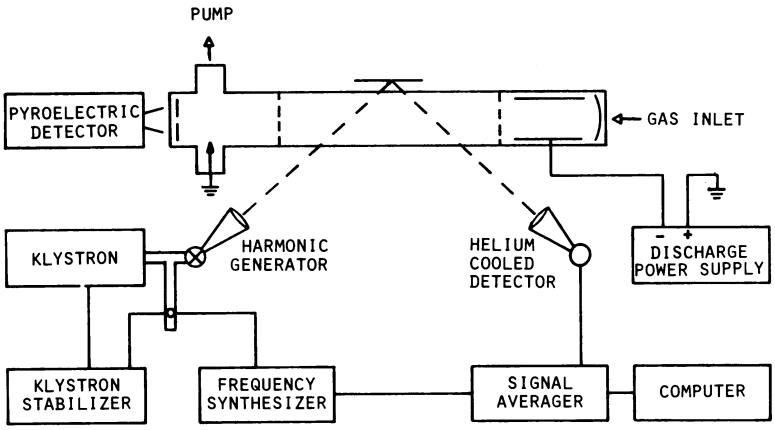

Fig. 3. Block diagram of the HCN discharge laser and millimeter/submillimeter diagnostic system. The fused quartz center section of the discharge tube is transparent to millimeter waves, allowing remote sampling of the positive column of the discharge plasma

significantly smaller uncertainties. From (1) the fractional change in the number density of a vibrational state is seen to be

$$\frac{n_1}{n_2}=\frac{T_1^2\Delta\nu_1\Delta P_1}{T_2^2\Delta\nu_2\Delta P_2}, \tag{2}$$

where the subscripts refer to measurements made under different discharge conditions (e.g., different currents). The uncertainty in this ratio is thus limited by how well the temperature and/or the area under the absorption line ($\propto\Delta\nu\Delta P$) are determined. These errors typically dictate an uncertainty of less than 10%.

For HCN there is another class of measurement that is independent of both temperature and pressure. Line Q's on the order of 10^6 and the sparse rotational spectra of linear molecules would normally dictate wide separation between rotational absorption frequencies of different vibrational states. However, serendipitous values of molecular constants for HCN result in lines that are quite close together ($\sim$70 MHz at $\sim$265 GHz) for several sets of different vibrational states. To first order the effective rotational constant for a linear triatomic molecule is [11]

$$B_{\text{eff}}=B_e-\alpha_1(v_1+\tfrac{1}{2})-\alpha_3(v_3+\tfrac{1}{2})-(\alpha_2\pm q_l/4)(v_2+1), \tag{3}$$

where B_e is the equilibrium rotational constant, the α_i are the vibrational expansion coefficients, the v_i are the respective vibrational quantum numbers, and q_l is the l-type doubling constant. Since $q_l=0$ for $l=0$, $q_l \cong 224$ MHz for $l=1$, and $\alpha_2=-108.37$ MHz [12], vibrational states m0^0n have rotational transition frequencies quite close to those of m1^{1c}n. A similar situation exists for states m2^0n and m1^{1d}n [c and d correspond to the plus and minus sign of q_l in (3)]. In addition $\alpha_1 \cong 300$ MHz and $\alpha_3 \cong 313$ MHz, so vibrational states mnp and (m$-$1)n(p$+$1) also have small separations between their rotational frequencies. These are extremely useful coincidences in that they allow a more accurate determination of population ratios between these vibrational states. From (1) this ratio is, to an excellent approximation,

$$\frac{n_1}{n_2}=\frac{\Delta\nu_1\Delta P_1[(J+1)^2-l_2^2]}{\Delta\nu_2\Delta P_2[(J+1)^2-l_1^2]}. \tag{4}$$

This equation is not rigorously correct because different vibrational states have slightly different dipole moments. The associated errors, however, are typically much less than 3%. The experimental uncertainty in measurements using (4) (often less than 5%) was determined by the signal/noise ratio of the absorption line.

3. Experimental

The millimeter/submillimeter microwave system used in this work was similar to those developed by the Duke Microwave Laboratory for spectroscopic purposes [13]. The output of a reflex klystron operating in the 35 GHz region was matched onto a crystal harmonic generator. The output of this generator, after lower harmonics were removed by waveguide filters, was transmitted via quasi-optical techniques through the laser plasma and detected by a 1.5 K InSb detector. The klystron was phase locked to a micro-processor controlled frequency synthesizer and the data collected in a digital signal averager. A laboratory computer was used for control and measurement purposes. The entire system, including the HCN laser and diagnostic spectrometer, is shown in Fig. 3.

The laser was 3.65 m long and 10 cm in diameter with the center section of fused quartz, which is transparent to mm waves, and end sections of pyrex. Two copper mirrors were used for the 3.6 m cavity. Laser power was monitored by a pyro-electric detector mounted behind a 0.25 cm diameter output coupling hole in the center

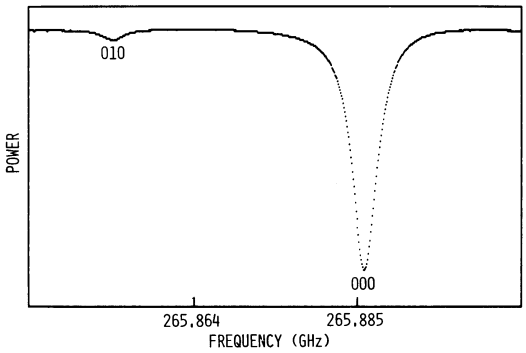

Fig. 4. Rotational absorption spectrum of the $J=3\leftarrow2$ transitions of the HCN 00^00 and $01^{1c}0$ vibrational states with a discharge current of 100 mA

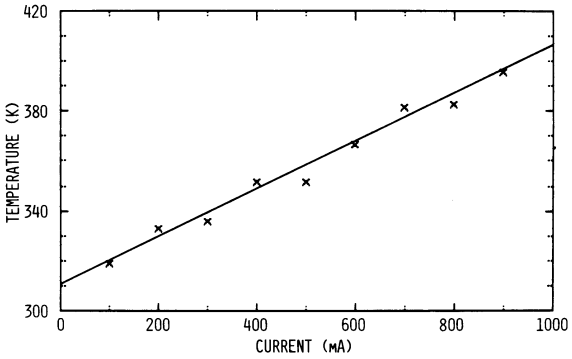

Fig. 5. Effective vibrational temperatures for HCN $01^{1c}0/000$ population ratios as a function of discharge current

of the 8.9 cm diameter plane mirror at the anode end of the discharge. The laser could be modulated at rates of several Hz by an electronic shutter (6.35 cm diameter aperture) mounted directly in front of this mirror. This facilitated the study of bottlenecking and competition effects. The other mirror was 7.6 cm in diameter with a 5 m radius of curvature. Both mirrors had micrometer tilt adjustment for cavity alignment, and the plane mirror was mounted on a micrometer translation stage for longitudinal mode selection.

The gas mixture was flowed into the cell through a hole behind the cathode mirror and pumped out through one arm of a T-section located next to the anode mirror. This arm also contained a capacitive manometer for pressure measurements. The other arm of the T-section contained a small stainless steel anode which was machined to a sharp point to enhance discharge stability. The cathode was 2.7 m from the anode and was constructed of a 50 cm long hollow stainless cylinder with an 8.9 cm diameter. The 0–4 KVDC, 2A discharge power supply was used in a positive ground configuration. The gas mixture, unless explicitly noted to be otherwise, was $N_2:CH_4=1:1$ for a total pressure of 200 mTorr and flow rate of 0.8 standard liters per minute. The discharge pressure varied between 210–230 mTorr with the current. The pressure, which is slightly less than typical pressures used by other researchers, produced narrower rotational absorption linewidths which were more amenable to our diagnostic technique.

4. Vibrational Temperatures

The near coincidence of rotational absorption lines for vibrational states differing by one bending quantum number greatly facilitated the demonstration of two fundamental aspects of the vibrational distribution of HCN in the discharge plasma. The ratios of the populations within the three bending stacks, 0n0, 1n0, and 0n1 were found to be given by the Boltzmann relationship with the same effective vibrational temperature (with relatively small deviations for higher bending states). In addition, this effective vibrational temperature was equal to the rotational/translational temperature of the neutral molecules in the discharge plasma.

Figure 4 shows the $J=3\leftarrow2$ rotational absorption spectrum for the 00^00 and $01^{1c}0$ vibrational states with a 100 mA discharge current. The population ratio of 24.8 determined from (4) and these data correspond to an effective vibrational temperature of 314 K. Figure 5 plots these temperatures as a function of discharge current. The plotted line is the least squares fit of these remarkably linear data. This curve is in fact predictable from a very simple model. In a normal glow discharge the energy input is proportional to the current. Thus, if the thermal conductivity dictated by the diffusion process remains unchanged, the change in temperature from the nearly ambient walls (the discharge was always run for short enough periods of time that the walls remained essentially at room temperature) should be proportional to the current.

The rotational spectrum in Fig. 6 contains absorption lines from the $01^{1c}1$, 00^01, $11^{1c}0$, and 10^00 vibrational states at a discharge current of 900 mA. These data were used as above to determine effective vibrational temperatures for the ratios $11^{1c}0/10^00$ and $01^{1c}1/00^01$. It was not possible to obtain accurate temperatures for currents less than $\sim$500 mA because of overlap between these lines in this current regime. This linewidth dependence on current is no doubt due to a peak in the concentration of polar molecules at $\sim$300 mA. Nevertheless, the temperatures obtained at the higher currents were the same, to within experimental uncertainties, for $11^{1c}0/10^00$, $01^{1c}1/00^01$, and $01^{1c}0/00^00$. For example, the temperatures derived from Fig. 6 are 416 and 428 K for $11^{1c}0/10^00$ and $01^{1c}1/00^01$, respec-

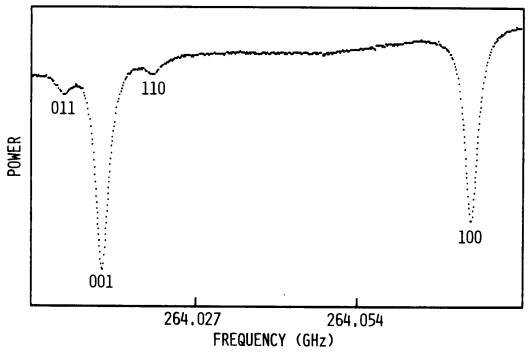

Fig. 6. Rotational absorption spectra of the $J=3\leftarrow 2$ transitions in the HCN $01^{1c}1$, $00^{0}1$, $11^{1c}0$, and $10^{0}0$ vibrational states with a 900 mA discharge current

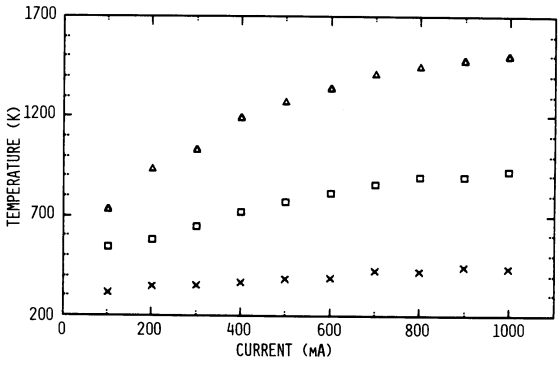

Fig. 7. Effective vibrational temperatures from the HCN 100/000 (□), 001/000 (△), and 020/010 (×) population ratios as a function of discharge current

tively. It should be noted that $11^{1c}0$ is the vibrational state containing the upper laser state. We have also investigated the $01^{1d}1$, $11^{1d}0$, and $01^{1d}0$ states and obtained similar results. Consequently we will assume the populations of the *l*-type doubling states are equal and omit the superscripts that differentiate between these states in most of the remaining sections.

Figure 7 shows the effective vibrational temperatures of 100/000, 001/000, and 020/010 as a function of discharge current. Since it was not possible to obtain the rotational line of 000 in the same klystron sweep as 100 and 001, (1) had to be used to determine their temperatures. The effective vibrational temperatures of 020/010 are seen to be nearly equal to those of 010/000 at low currents. They are slightly hotter at higher currents, with this deviation increasing with current. It is important to note that this difference in temperature between 020 and 010 is quite small in comparison to the very non-thermal temperatures exhibited by 100 and 001. Comparison with 100 is especially germane because the upper lasing state 110 is the first vibrational state in the bending stack built upon this fundamental stretching mode. The increase in temperature for the higher bending overtones is not a surprising result since the molecules cascading down a bending stack will make relatively larger contributions to the smaller populations of the higher bending states. The number of HCN molecules in highly excited vibrational states increases with current so this cascading effect would make a larger difference at higher currents.

The ratio of the population of 010 to 000 must be greater than or equal to that given by the Boltzmann equation with the rotational/translational (R/T) neutral gas temperature since the existence of a mechanism that would selectively depopulate 010 and not 000 is extremely unlikely. Consequently, the effective vibrational temperature of 010/000 is an upper bound on the R/T temperature. With a 50 mA discharge current the outside tube temperature remains essentially at room temperature even after extended periods of operation so the zero current value of $T=310$ K from Fig. 4 indicates that the effective vibrational temperature equals the R/T temperature. Although it might be argued that this thermal equilibrium is an inevitable result of the low discharge current it should be noted that even with a current as low as 100 mA some vibrational states have very non-thermal populations. For example, 100 and 001 have populations 30 and 330 times larger than they would if they were in 320 K thermal equilibrium with 000. The equality of the effective vibrational temperatures derived from all three ratios, 010/000, 110/100, and 011/001 provides further evidence that the bending stacks are in thermal equilibrium. The non-thermal excitation and relaxation processes for 110, 011, and 010 must certainly have different rates. This would lead to different effective vibrational temperatures for these states unless the rate for the thermal equilibration of the bending stacks is much faster and thus rate determining. In addition, thermometry measurements of the neutral gas temperature [5] are in satisfactory agreement with our temperatures when the differences in gas mixture, pressure, and current density are taken into account. For these reasons, we are quite confident that these effective vibrational temperatures are equal to the R/T gas temperature. This thermal equilibrium among the states in a bending stack provides a significant reduction in the number of degrees of freedom in models of vibrational excitation. It also provides an R/T temperature calibration; allowing absolute concentrations to be calculated via (1).

5. Bottlenecking and Competition Effects

It is well known that vibration-vibration exchange processes such as HCN(000)+HCN(020) $\rightleftarrows$2 HCN(010) allow bending state equilibration to occur at rates much faster than those which result from relaxation processes such as HCN(100) $\rightarrow$HCN(000). This has been recognized in the literature as being beneficial to creating and sustaining a population inversion between the lasing states [6]. It tends to increase the population in the upper lasing state by giving it access to the large population stored in 100 and also promotes rapid relaxation of the lower lasing state into the bending modes below it. Since vibration-vibration exchange processes like the above are not able to relax the 010 state there has been some conjecture [6] that this bottleneck may cause a high effective vibrational temperature for the bending modes, thereby reducing the inversion between the lasing states. The rapid rate of exchange between 000 and 010 that is necessary to maintain the demonstrated thermal equilibrium between these states and the R/T temperature would make it difficult for a bottleneck in 010 to exist.

Bottlenecking, if present, would be most severe during strong laser oscillation and would result in a significant difference between the lasing and non-lasing population of 010. The electronic shutter mounted in front of the anode end mirror allowed sensitive comparisons of these populations to be made under virtually identical discharge conditions. No measurable change in the population of 010 was found, even with the strongest laser intensity. The experimental uncertainty of these ratios, which were calculated by (2) with $T_1 = T_2$, was about 2%. The absence of bottlenecking in 010 indicates that the relaxation of 010 (and all the non-zero bending modes within a given bending stack) is dominated by non-resonant vibration-translation and/or vibration-rotation exchange processes. McGarvey et al. [14] have used laser induced fluorescence techniques to determine a probability of $\lesssim$0.011 for HCN(000)+HCN(010)$\rightarrow$2 HCN(000). This self-deactivation process, being non-resonant, should have approximately the same probability as those for the relaxation of HCN(010) through collisions with other molecular species in the discharge plasma. These large rates are consistent with both the demonstrated thermal equilibrium and absence of bottlenecking.

The thermal equilibrium between states in a bending stack also implies tight coupling between 100 and 110. This suggests that 100 should exhibit laser induced competition effects since some of the population removed from 110 by stimulated emission would be rapidly replaced by molecules residing in 100, thus decreasing the population in 100. Measurements of the population of 100 as a function of laser intensity (implemented in the same manner as was used in checking for bottlenecking in 010) confirmed the presence of a small, but experimentally unambiguous, competition effect. While lasing, the populations in 100 at currents of 800, 900, and 1200 mA were found to be smaller by 2%, 3.5%, and 4%, respectively, than the populations under the same discharge conditions with the laser not oscillating. The estimated experimental uncertainty of the population ratios is 0.5%. This is smaller than the above uncertainties in the ratios for 010 because at the high currents necessary for intense laser oscillation 100 has a larger population, and hence better signal to noise ratios, than 010. The millimeter wave probe beam has a cross sectional diameter of $\sim$5 cm and, in the probed section of the positive column of the discharge, 90% of the laser intensity is contained in a cross sectional area with a diameter of $\sim$3.6 cm (Sect. 7). Consequently, given the 10 cm diameter of the discharge tube, approximately 1/4 of the molecules sampled by the millimeter wave probe are in the laser beam. Thus, the competition effect is actually $\sim$4 times greater than the experimental ratios indicate.

6. Absolute Vibrational State Concentrations

Figure 8 shows the number density of HCN(000) as a function of discharge current. These absolute concentrations were derived from (1) with the R/T temperature determined from Fig. 5. HCN, which exists predominantly in its ground vibrational state, was a small constituent of the total gas pressure. Even at its peak concentration near 250 mA the partial pressure of HCN was only 7.1 mTorr out of a total gas pressure of 230 mTorr and at 1 A it had dropped to 2.6 mTorr. Comparison of the number density of HCN(000) with the laser output power, which is also plotted in Fig. 8, shows that ground vibrational state HCN peaks at a current substantially less than the peak laser power current. This is in qualitative agreement with the results of mass spectroscopy measurements made by Schötzau and Kneubühl [15]. The peak in the laser power at a current significantly greater than that at which the HCN(000) concentration peaks is in itself unremarkable since the concentrations of excited vibrational states would also be expected to have maxima at higher currents.

The number densities of HCN(100) and (001) from Fig. 9 show that these excited vibrational states do in fact peak at higher currents. Comparison of Figs. 8 and

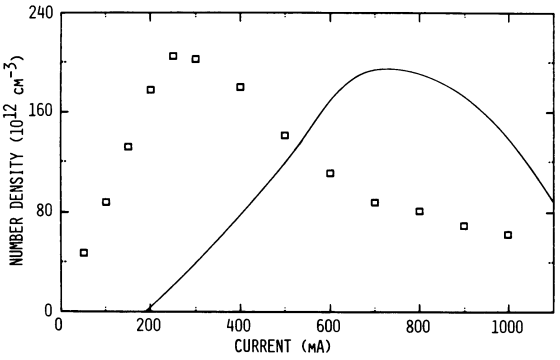

Fig. 8. HCN 000 vibrational state number density as a function of discharge current. The solid line is the laser output power in arbitrary units

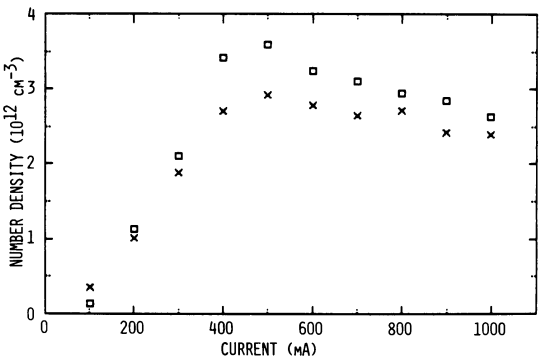

Fig. 9. HCN 100 (×) and 001 (□) vibrational state number densities as a function of discharge current

9 again demonstrates (as does Fig. 7) that 100 and 001 have very non-thermal populations. With comparable sensitivity and integration time we did not detect the rotational absorption for the lower laser state HCN(040) whereas a relatively strong absorption for the upper state HCN(110) was obtained, thus showing a large lasing inversion.

Some of the possible excitation schemes hypothesised in the literature result in the production of HCN primarily in asymmetric vibrational states. This would require tight asymmetric-symmetric mode coupling to transfer the molecules to the upper lasing state. In addressing this issue, Pichamuthu [6] has suggested that collisional (asymmetric mode) ↔ (symmetric mode) interconversions may occur very rapidly, resulting in thermal equilibrium between 001 and 100. Figure 9 shows this is clearly not the case since these states have nearly the same populations even though 001 is more than 1000 cm^{-1} above 100. This corresponds to a very significant deviation from equilibrium; from Fig. 7 the population of 001 is seen to be in excess of two orders of magnitude larger than it would be if it were in equilibrium with 100.

As we pointed out in an earlier paper on the HCN discharge plasma [16], the near equality of the populations of 100 and 001 show that the metastability of 100 is not a necessary pre-requisite for obtaining the lasing inversion (as has often, at least implicitly, been assumed). Thus, vibrational states that are coupled to a lower state by an irregular perturbation (which is a fairly ubiquitous occurrence in polyatomic molecules) are still potential lasing candidates even if they are not radiatively metastable. This substantiates Robinson's statement [17] that the dearth of far-infrared discharge lasers (virtually all of which depend on perturbation mixing) is probably due to the proclivity of polyatomic molecules towards rapid dissociation under discharge conditions. Isotopically substituted molecules have similar chemical and dissociation properties but have wholly different vibrational levels and perturbations. Thus, the fact that most isotopes of FIR discharge lasing molecules will also lase provides additional evidence that the paucity of FIR discharge lasers is due primarily to dissociation rather than a lack of coincidences between appropriate vibrational population distributions and irregular perturbations.

7. Laser Gain and Threshold

Our data allow a straightforward calculation of the laser gain, which at the threshold current of 200 mA (Fig. 8) should equal the cavity losses. The gain of the primary, ($11^{1c}0$, $J=10$)→($04^{0}0$, $J=9$), lasing transition is [10] (assuming total inversion)

$$\gamma = \frac{2.16\times 10^{8}\exp(-233/T)Pb^{2}}{T^{2}\Delta\nu}\,\mathrm{cm}^{-1}, \qquad (5)$$

where T is the R/T gas temperature [K], $\Delta\nu$ the HWHM linewidth [MHz], P the partial pressure of the upper vibrational state [Torr], and b^2 the square of the Coriolis mixing coefficient. At a 200 mA discharge current, the number density of 100 (Fig. 9) along with the temperature (Fig. 5) and thermal equilibrium between 110 and 100 give a partial pressure of 1.5 μTorr for 110. At this current, the linewidth is 1.9 MHz for the 100 $J=2\rightarrow3$ transition. This should change by a relatively small amount for $J=9\rightarrow10$ and would also be expected to be nearly the same for the nearby 110 vibrational state. The actual linewidth is larger due to the convolution with the Doppler width of 1.1 MHz at this frequency and temperature. An effective width of 2.2 MHz correctly accounts for both this broadening and also the resulting deviation of the lineshape from Lorentzian [which is assumed in deriving (5)]. These

numbers, along with the Coriolis mixing coefficient of 0.13 from Maki and Blaine [18], give $\gamma = 8.7 \times 10^{-5}\,\mathrm{cm}^{-1}$. A round trip gain of 4.4% is then obtained from the positive column length of 255 cm.

For oscillation in its fundamental mode, the electric field of the laser radiation has a Gaussian profile determined by the geometry of the resonator cavity [19]. The resulting spot sizes (1/e radii) of 1.55 cm and 2.43 cm at the plane and spherical mirrors, respectively, and a simple numerical integration then lead to the following cavity losses: 0.8% through the output coupling hole, $<0.01\%$ from diffraction around the aperture in front of the plane mirror, and 1.7% from diffraction around the spherical mirror. From classical Electricity and Magnetism theory the reflectivity loss is given by $(8\varrho\varepsilon_0\omega)^{1/2}$ (where ϱ is the resistivity of the mirror, ε_0 is the electric permitivity and ω the angular frequency of the incident radiation), which for copper mirrors at 840 GHz is 0.26%. The resulting net round trip loss of 3% is only 1/3 less than the computed gain, an excellent agreement. Neglected cavity loss mechanisms, such as decreased reflectivity due to dirty mirrors, scatter, or losses from imperfect alignment are the principal reasons for this difference. These results provide further evidence that the parameters and assumptions used in (5) are essentially correct.

The widely reported [20, 40, 41] dependence of the output power of cw HCN lasers on the wall temperature of the discharge tube can be explained, in a fairly quantitative manner, on the basis of the demonstrated thermal equilibrium between the 100 and 110 vibrational states. This equilibrium, in conjunction with the assumptions that the partial pressure of 100 and the linewidth are relatively insensitive to temperature changes in the region of interest (these assumptions are supported by our data), results in the following proportionality for the gain coefficient: $\gamma \propto T^{-2} \exp(-1240/T)$, which has its maximum value for $T = 620$ K. Belland and Veron have measured [20] an optimum inner wall temperature of ~ 390 K for $N_2 : CH_4$ gas mixtures with a discharge current $\lesssim 1$ A. In similar gas mixtures, but slightly lower currents, Schötzau and Kneubühl have reported [21] axial temperatures of 490–560 K in conjunction with wall temperatures of ~ 400 K. This indicates that the axial temperature corresponding to the Belland and Veron inner wall temperature of ~ 390 K (the axial temperature being germane since the 1/e radius of their laser mode was 0.7 cm) was quite close to our derived optimum temperature of 620 K.

8. Excitation Mechanisms

There exist a number of excitation mechanisms that are operative in gas laser systems [22]. Those that are potential candidates for the HCN discharge laser can be classified as direct charged-particle (usually electrons) excitation, chemical reactions, and resonant vibrational energy transfer. Experimental evidence that directly supports a particular mechanism has been difficult to obtain. On the basis of the laser inactivity of cw discharges in pure HCN as opposed to the stimulated emission observed in pulsed discharges and the concurrent decrease in HCN concentration and increase in laser intensity with each current pulse, Schötzau and Kneubühl [15] have concluded that electron impact is not the principal excitation mechanism.

The general consensus [5, 6, 17, 23] has been that the chemical reaction

$$CN + H_2 \rightarrow HCN^* + H \tag{6}$$

is the dominant pumping mechanism in discharge lasers; however, the experimental evidence for this is not conclusive and, to a great extent, is based upon arguments by elimination. Our measurements of the absolute concentration of CN in cw discharge plasmas indicate that the partial pressure of CN is several orders of magnitude smaller than would be necessary for this reaction to produce quantities of excited state HCN sufficient for observed laser intensities.

Resonant energy transfer (specifically vibrational transfer from $N_2(v=1)$ to HCN(100) in a manner entirely analogous to the well known CO_2 laser pumping scheme) has received little attention in the literature. It is not possible directly to measure concentrations of N_2 molecules by our technique since N_2 has no permanent electric dipole moment and hence no pure rotational absorption spectra. However, several attributes of a variety of vibrational state concentration measurements performed on HCN and CO (which can be included in the gas mixture to provide an indirect measure of the N_2 vibrational distribution) indicate that this near resonant vibrational transfer may well be the predominant excitation mechanism in cw discharge systems.

8.1. Chemical Excitation

Pichamuthu [6] has argued that in discharge lasers the ground electronic state of the CN radical, CN(X), is the most likely candidate for chemical pumping via reaction (6). We have measured in situ the number density of the ground vibrational state of CN(X) as a function of current. This is plotted in Fig. 10. Even at its peak, the concentration is only 6×10^{-6} Torr. Although the details of the processes that would eventually convert this CN concentration into laser power are not well determined, it is possible to do several limiting calculations to show the difficulty of

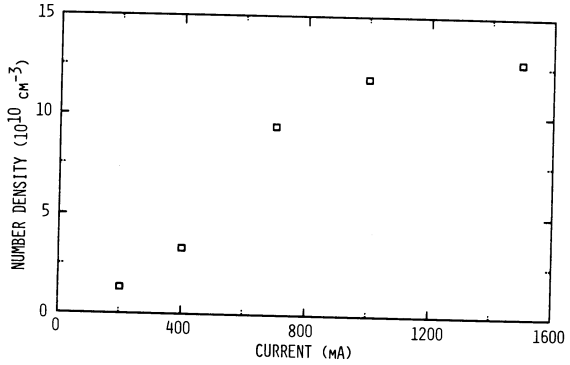

Fig. 10. $X^2\Sigma^+$ CN number density as a function of discharge current

accounting for the observed properties of this system via processes of the type proposed in (6). Under the most optimistic assumption that all of the CN that is converted by (6) into excited state HCN passes through the state HCN(110) we have

$$\frac{N\{\mathrm{HCN}(110)\}}{N\{\mathrm{CN}\}} = \frac{T\{\mathrm{HCN}(110)\}}{T\{\mathrm{CN}\}}, \tag{7}$$

where the T's are the lifetimes and the N's the number densities.

A simple but somewhat subtle argument based on the Coriolis perturbation and pressure broadened linewidth can be used to find $T\{\mathrm{HCN}(110)\}$. The lifetime of a rotational state, $t = 1/2\pi\Delta\nu$ where $\Delta\nu$ is the pressure broadening contribution to the pure rotational transition linewidth, is due almost entirely to rotationally inelastic collisions [39] (primarily $\Delta J = \pm 1$). We have measured $\Delta\nu \cong 1.9$ MHz which gives a lifetime of 8.4×10^{-8} s from these J changing transitions. Since the square of the Coriolis mixing coefficient between the $J = 10$ levels of HCN(110) and HCN(040) is 0.13 [18] the molecules in $J = 10$ HCN(110) will undergo transitions to HCN(040) at about 0.13 of this rate. Furthermore, the population in $J = 10$ comprises about 1/16 of the total population of the vibrational state so the entire rotational manifold in HCN(110) will have a lifetime of $T\{\mathrm{HCN}(110)\} = (8.4 \times 10^{-8})$ (16) (1/0.13) $\cong 10\,\mu$s. This is much faster than normal vibrational exchange rates and consequently must be the rate determining process.

Upper state lifetimes have also been derived from Q-switched experiments. Yamanaka et al. [25], and Jones et al. [26] reported times of approximately 6 μs whereas Frayne [27] obtained a value of about 120 μs. This apparent disparity is due to the fact that the effective upper states being measured were not the same and actually, with the proper interpretation, all three are consistent with our value of 10 μs. Yamanaka et al., and Jones et al. determined the lifetime from the ratio of the Q-switched and cw peak powers. Their Q-switched laser pulses were several μs long which is of sufficient duration to allow the majority of the rotational states in HCN(110) to contribute to the stimulated emission. Therefore their lifetimes correspond to that of the entire vibrational state and are seen to be in excellent agreement with our computed value. Frayne, on the other hand, obtained the upper state lifetime from measurements of the fractional change in peak Q-switched power between two successive pulses. Since the time between pulses was relatively long (~1 ms), molecules initially in HCN(100) will contribute significantly to the population of HCN(110) on this time scale. Consequently the measured effective lifetime was that of the coupled HCN(110), HCN(100) system. Frayne's results can be shown to be consistent with the interaction between these vibrational states and $T\{\mathrm{HCN}(110)\} = 10\,\mu$s. This topic, along with supporting quasi-cw pulsed decay data, will be discussed in detail in a later paper.

West [24] has measured the rate for (6) to be 2×10^{-14} cm^3 mol^{-1} s^{-1} which at a H_2 pressure of 200 mTorr gives $T\{\mathrm{CN}\} \cong 7$ ms. This value, along with $T\{\mathrm{HCN}(110)\} = 10\,\mu$s, then obtains a population ratio of 1.4×10^{-3} from (6). Our directly measured ratio of about 3 is more than a factor of 1000 greater, mitigating quite strongly against the reaction of (6). It could be argued that the rate constant of West should be increased because our discharge is at an elevated temperature. However, it is also true that only a fraction of HCN* will pass through 110.

An alternative calculation that does not use the lifetime of HCN(110) is possible. This calculation is based on the output power of the HCN laser. By use of the same rate constants, concentrations, the volume of our resonator, and the assumption that every CN species that participates in the process of (6) contributes a laser photon, it is straightforward to calculate that our laser would produce at most 50 μW from this source. Although we have not made absolute measurements of our laser output power, a conservative lower limit estimate can be obtained from a compilation of reported output powers per resonator volume [5]. Even the smallest of these (they range from 0.4–11.8 mW liter^{-1}) predicts a cw power of ~10 mW for our system. Thus, although there are substantial uncertainties in both directions in these calculations, it would appear that the CN concentration is too small by a factor of 100–1000 in our system to account for its excitation and power via the reaction of (6).

Wall deposits from discharge contaminants affect laser power in two distinct ways. The formation of a brown polymer that is found to occur with many gas mixtures and operating temperatures tends to reduce the laser output power [20]. Under other circumstances wall

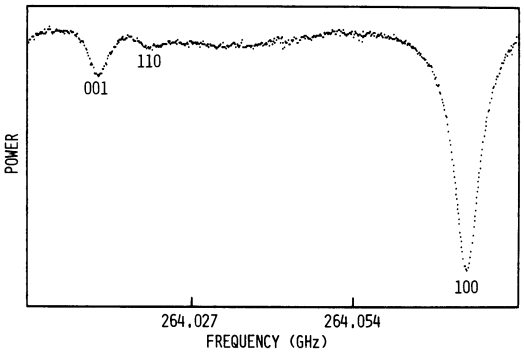

Fig. 11. Rotational absorption spectra of the $J=3\leftarrow 2$ transition in the HCN 011, 001, 110, and 100 vibrational states with the CO admixture and 300 mA discharge current

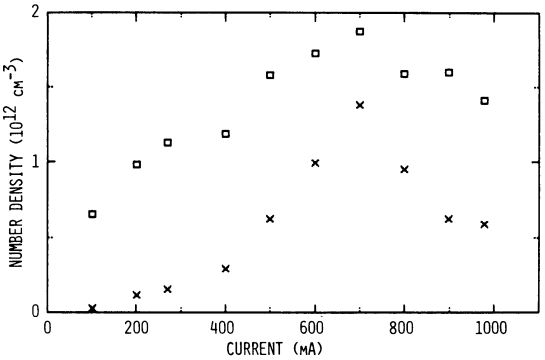

Fig. 12. HCN 100 (□) and 001 (×) vibrational state number densities as a function of discharge current with the CO admixture

deposits appear to be potentially beneficial. There have been numerous reports [28, 29] of laser oscillation, at reduced powers, in discharges of pure H_2 after appropriate wall deposits have accumulated from standard mixture discharges. Kunstreich and Lesieur [23] have even reported laser operation from wall deposits with mixtures of H_2+N_2 with powers as high as those obtained with normal gas mixtures and lasting for periods up to 15 minutes after the termination of the flow of the carbon containing molecule [CH_4 or $(CN)_2$]. One interpretation of these results is CN or HCN* may be formed on the wall. Another possibility is that the wall may merely function as a source of carbon or nitrogen containing molecules for subsequent gas phase reactions. Under typical discharge conditions the time for diffusion from the wall into the laser mode volume is ~ 10 ms from basic kinetic transport theory. As discussed above, the effective lifetime of the upper laser state of HCN (including relatively long term contributions from vibrational states other than 110) is about 100μs. Thus, even if HCN* were formed on the walls, it would not be able to contribute to the stimulated emission. This argument remains valid even for waveguide lasers (which allow the largest filling factor) since the lowest loss modes in these systems have diameters of about half that of the discharge tube. Due to the above considerations it would appear unlikely that the excitation we observe in our cw discharge laser system is provided primarily by a chemical reaction.

8.2. Near Resonant Vibrational Energy Transfer

The first report of the effect of CO on cw HCN discharge lasers was made by Dyubko and Topkov [30]. They found that the addition of CO to standard gas mixtures reduced the threshold current, resulting in an enhancement of laser power at low currents and reduction at high currents. They suggested that the enhancement may be due to vibrationally excited CO pumping HCN via the near resonant transitions, $CO(v=1)+HCN(000)\rightarrow CO(v=0)+HCN(100)+46\,cm^{-1}$ and $CO(v=1)+HCN(010)\rightarrow CO(v=0)+HCN(110)+51\,cm^{-1}$. Upon the inclusion of 200 mTorr of CO in our standard mixture (for $CH_4:N_2:CO=1:1:2$ with a total pressure of 400 m Torr) we found threshold and power changes similar to those described by Dyubko and Topkov.

Vibrational state population measurements of CO and HCN in the above admixture were significant to the understanding of excitation mechanisms. The rotational spectrum shown in Fig. 11 was taken with this gas mixture at a 300 mA discharge current. The decrease in the population of 001 relative to 100 demonstrated by this spectrum (Fig. 6) also existed at all other discharge currents. It should be noted that thermal equilibrium among vibrational states in a given bending stack was maintained with this admixture. For the particular case illustrated by Fig. 11, this resulted in the rotational absorption line of 011 dropping below the noise level since 011 is in equilibrium with the diminished 001 population. The R/T temperatures derived from 010/000 ratios with the CO admixture were not substantially different from those obtained with our standard gas mixture. Fig. 12 plots the number densities of the 100 and 001 vibrational states computed from (1) and these temperatures. Comparison with Fig. 9 shows that the population of 001 is greatly reduced by the addition of CO, especially at low discharge currents. The population in 100, although it is also reduced at higher currents, is seen to be enhanced at currents less than 200 mA. This is consistent with the noted change in laser gain in these two current regimes.

Very substantial population densities of vibrationally excited N_2 are readily obtained in low pressure discharges (it is estimated that 10–30% of the N_2 in a discharge may exist in excited vibrational states [31])

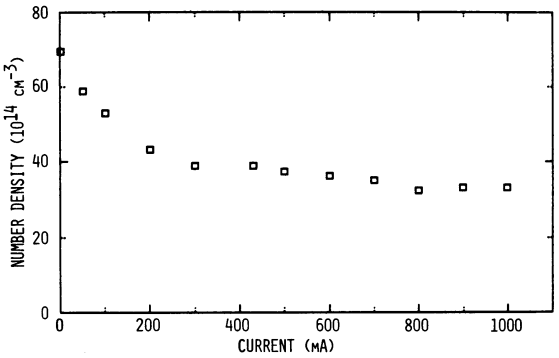

Fig. 13. Number density of the ground vibrational state of CO as a function of discharge current

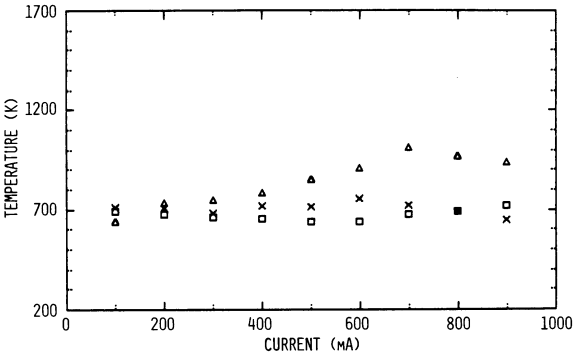

Fig. 14. Effective vibrational temperatures from the HCN 100/000 (□), 001/000 (△), and CO $v=1/v=0$ (×) population ratios as a function of discharge current. The experimental uncertainty in these temperatures is approximately 50 K

owing to this molecule's large cross section for electron impact excitation and high immunity to dissociation. CO is isoelectronic with N_2 and consequently also has a large cross section for this vibrational excitation mechanism. Schulz [32] has used a double electrostatic analyzer to measure peak total vibrational cross sections of $3\times10^{-16}\,\mathrm{cm}^2$ and $8\times10^{-16}\,\mathrm{cm}^2$ for N_2 and CO, respectively. Near resonant vibrational transfer via $N_2(v=1)+CO_2(000)\rightarrow N_2(v=0)+CO_2(001)$ $-18\,\mathrm{cm}^{-1}$ is known to be very effective in pumping discharge CO_2 lasers because of its rapid rate [33] ($\sim1.9\times10^4\,\mathrm{Torr}^{-1}\,\mathrm{s}^{-1}$) and the abundance of $N_2(v=1)$. Similarly, vibrational energy transfer by $N_2(v=1)+HCN(000)\rightarrow N_2(v=0)+HCN(100)$ $+233\,\mathrm{cm}^{-1}$ [and the equivalent transition involving $CO(v=1)$ when this gas is included in the mixture] would be expected to be the primary excitation mechanism for cw HCN discharge lasers. This is an attractive hypothesis both because of the similarities between the relevant energy levels and discharge conditions in the CO_2 and HCN systems and because this model provides a straightforward explanation of several features of our data.

The energy defects of 233 and $46\,\mathrm{cm}^{-1}$ for the $HCN(100)/N_2(v=1)$ and $HCN(100)/CO(v=1)$ near resonances are significantly greater than the $18\,\mathrm{cm}^{-1}$ difference for the $CO_2(001)/N_2(v=1)$ resonance. However, both these values are near kT (which is approximately the "width" of these resonances). Furthermore, although the equivalent $CO_2(001)/CO(v=1)$ resonance has an energy defect of $206\,\mathrm{cm}^{-1}$, its measured rate constant [34] of $0.79\times10^4\,\mathrm{Torr}^{-1}\,\mathrm{s}^{-1}$ is only a factor of 2.4 less than that of the $CO_2(001)/N_2(v=1)$ resonance. Thus, the $HCN(100)/N_2(v=1)$ and $HCN(100)/CO(v=1)$ energy defects are small enough not to preclude a similarly large rate constant.

The vibrational transfer model could account for the observed low current enhancement of the population of HCN(100) on the basis of the difference in the energy defects of N_2 and CO. At low discharge currents CO might be expected to be more efficient than N_2 in populating HCN(100) by this near resonant transfer mechanism because the energy defect for CO is $\sim1/4\,kT$ whereas the defect for N_2 is slightly larger than kT. This difference in the energy defects would be less significant at higher currents where kT is larger.

Our measured HCN(100)/HCN(000) population ratios are typically 3%. This is consistent with the proposed vibrational transfer mechanisms and estimated $N_2(v=1)/N_2(v=0)$ ratios. The CO admixture provides a means of quantifying this relationship. Vibrational state populations of CO and N_2 would be expected to be essentially in equilibrium in discharges containing these molecules because of the similarities in their excitation processes, their long vibrational lifetimes, and the rapid rates associated with vibrational exchange transitions such as $CO(v=1)$ $+N_2(v=0)\rightleftarrows CO(v=0)+N_2(v=1)$. Consequently, a correlation between $CO(v=1)/CO(v=0)$ and HCN(100)/HCN(000) would be anticipated on the basis of the proposed excitation mechanism.

Figure 13 shows the measured ground state CO number densities as a function of discharge current. The zero current number density of $68\times10^{14}\,\mathrm{cm}^{-3}$ corresponds to a partial pressure of 224 mTorr. This is in good agreement with the 200 mTorr value obtained from pressure measurements and is an indication of the level of uncertainty in absolute concentrations obtained from our rotational absorption measurements. Similar measurements of $CO(v=1)$ showed a monotonic decrease in number density for discharge currents greater than 50 mA. The effective vibrational temperatures determined from the ratios of $CO(v=1)/CO(v=0)$, HCN(100)/HCN(000), and HCN(001)/HCN(000) are shown in Fig. 14. These ratios were obtained under virtually identical dis-

charge conditions and consequently are independent of the R/T gas temperature. The CO admixture significantly changes the effective vibrational temperatures of HCN(100)/HCN(000) and HCN(001)/HCN(000) (Fig. 7). This is unremarkable in and of itself; however, the equality (to within experimental uncertainty) of the $CO(v=1)/CO(v=0)$ and HCN(100)/HCN(000) temperatures is quite salient. It not only provides strong evidence supporting the near resonant vibrational transfer mechanism, but it also indicates that this mechanism is so fast as to dominate all of the decay mechanisms available to HCN(100).

Our data do not provide an unambiguous explanation of the concentrations and effects observed for the HCN(001) population. They do, however, suggest several plausible mechanisms. H_2, like CO and N_2, has a fairly large cross section for vibrational excitation by direct electron impact [32]. Mass spectroscopy measurements [15] have shown large concentrations of H_2 in HCN discharge plasmas. Consequently, since $H_2(v=1)$ is only 157 cm^{-1} above HCN(011) [which is tightly coupled to HCN(001)], near resonant vibrational transfer between these vibrational states might be expected to result in concentrations of HCN(001) consistent with our measurements. Another, not necessarily mutually exclusive scenario, is that vibrational transfer between $N_2(v=2)$ and HCN(021) (53 cm^{-1} energy defect) may be feeding HCN(001). If the population in $N_2(v=2)$ corresponds to the same vibrational temperature as that of $N_2(v=1)$ (Raman spectroscopy measurements [35] have demonstrated that this is the case in discharge excited $CO+N_2$ mixtures, albeit at higher pressures), then equilibrium between $N_2(v=2)$ and HCN(021) would predict a HCN(001) population ~ 5 times larger than observed. This is actually a reasonable deviation since the relatively large changes in vibrational quantum numbers for this transfer might be expected to result in a rate that is too slow to equilibrate these states.

The observed large reduction in the population of HCN(001) with the CO admixture is also amenable to explanation on the basis of higher-order vibrational transfer. $CO(v=2)$ is most nearly resonant with HCN(011) (energy defect of 256 cm^{-1}) rather than HCN(021) as for $N_2(v=2)$. Thus, equilibration via vibrational transfer with $CO(v=2)$ predicts a smaller HCN(001) population than would result from the equivalent $N_2(v=2)$ transfer. Although the magnitude of the calculated depletion is a factor of ~ 3 larger than was observed, this is again a reasonable deviation since the contribution of $N_2(v=2)$ has been ignored.

Our data do not preclude the previously discussed chemical reaction from being a major contributor to the HCN(001) population. However, mitigating evidence is provided by the Flournoy and Nelson demonstration [36] of collisional excitation of HCN by energy transfer with vibrationally hot diatomic molecules. They flowed discharge excited N_2, H_2, and D_2 into pure HCN and observed the resulting HCN ν_3 fundamental ($001 \rightarrow 000$) emission spectra (N_2 producing the largest emission). These authors noted that vibrationally excited HD produced less HCN(001) emission than N_2, H_2, or D_2, even though $HD(v=1)$ has the smallest energy defect with HCN(001). They felt that this was an anomalous result in that it suggests that the vibrational energy transfer is not necessarily resonant which conflicts with the rest of their experimental evidence. Our proposed resonant vibrational transfer mechanisms for the excitation of HCN(001) would resolve this apparent anomaly since they involve resonant transfer to HCN(011) and HCN(021) [which have small energy defects with $N_2(v=2)$ and $H_2(v=2)$ but not with $HD(v=2)$] and subsequent transfer to HCN(001) via the rapid equilibration of the bending stack.

It should be noted that these results of Flournoy and Nelson not only support our conjectured HCN(001) excitation mechanisms but they also provide additional evidence for the veracity of our HCN(100) excitation mechanisms. This is because the single quantum vibrational exchanges required to excite HCN(100) must certainly be more efficient than the multi-quantum exchanges needed for the demonstrated excitation of HCN(001). They did not observe an emission from HCN(100) because the transition moment from this state is very small.

8.3. Overview of Vibrational Temperature

Because of the large number of states and species involved, it could be argued that a more global approach is appropriate. From the above, we conclude that the following are important components of such an approach:

1) In a discharge, vibrational exchange processes of the form

$$N_2(v=1)+N_2(v=1)\rightarrow N_2(v=0)+N_2(v=2) \qquad (8)$$

are very rapid and make possible the description of the populations of many excited states by a single temperature.

2) Because of the near resonances among $CO(v=1)$, $N_2(v=1)$, and HCN(100) or $H_2(v=1)$ and HCN(011), a single temperature may be used to describe a family of modes in several species.

3) The bending modes of HCN are of much lower energy than the stretching modes and are basically in thermal equilibrium with the R/T temperature.

4) Because the processes described in (1–3) are not infinitely fast and the excitation energy is injected at

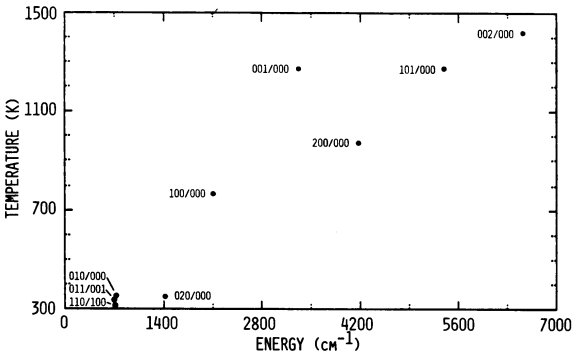

Fig. 15. HCN effective vibrational temperatures as a function of vibrational energy difference with a 500 mA discharge current

relatively high energy, the cascading down the vibrational energy ladders causes the higher levels to be somewhat hotter than the lower levels.

5) Although energy resonances exist between states like $N_2(v=1)$, HCN(100), and HCN(030), the probability of energy exchange with HCN(030) is relatively small because the vibrational states are substantially different. This prevents the bending modes from equilibrating the stretching modes at the R/T temperature.

Figure 15 shows the vibrational temperatures for the HCN 010/000, 110/100, 011/001, 020/000, 100/000, 200/000, 001/000, 002/000, and 101/000 population ratios with a discharge current of 500 mA. It can be seen that the bending modes are near the R/T temperature of 360 K. The stretching modes are all substantially hotter than this. With the exception of 001, which was discussed above, the temperature of these stretching modes increases smoothly with energy. In the interpretation of this graph, it must be remembered that a relatively small amount of excess cascading population will make a substantial increase in temperature at the higher energies because the "thermal" population is so small. Although, in principle, the vibrational excitation shown in this figure depends only upon the rapid exchange of energy and could be driven by electron impact, chemical processes, or vibrational exchange, our results strongly indicate that the energy initially deposited in N_2 and CO is the dominant contributor.

8.4. Laser Efficiency

HCN discharge lasers have efficiencies on the order of 10^{-4} which, especially in comparison with CO_2 laser efficiencies of $\sim 10^{-1}$, appear to be quite small. Basic physical considerations, however, show that this efficiency is actually surprisingly large and indicate that a substantial fraction ($\sim 10\%$) of the HCN molecules in excited vibrational states decay via the stimulated emission path [37]. Our competition effect measurements show that approximately 10% of the molecules in HCN(100) participate in the stimulated emission. The population of 100 comprises about 40% of the excited-vibrational-state population of HCN so $\sim 4\%$ of the vibrationally excited HCN decays via stimulated emission [this is actually a lower bound since HCN molecules initially excited into higher vibrational states may decay to HCN(100) or HCN(110)]. This is in reasonable agreement with the conjectured 10%.

Comparison of HCN and CO_2 laser efficiencies is particularly germane in view of our proposed excitation mechanism. If the HCN discharge laser is indeed primarily pumped by near resonant vibrational transfer from vibrationally excited N_2, as the CO_2 laser system is, then a direct correlation between the efficiencies of these lasers might be expected. The HCN efficiency would have the same factor of $\sim 10^{-1}$ as the CO_2 laser to account for the nitrogen excitation and the other energy expenditures in the glow discharges. The HCN efficiency would contain an additional factor of $\sim 3 \times 10^{-3}$; 3×10^{-2} of this being due to the difference in photon energy and the other factor of 10^{-1} resulting from the fact that only $\sim 10\%$ of the HCN(100) molecules contribute to the stimulated emission. Considering the simplicity of this calculation, the derived net efficiency of $\sim 3 \times 10^{-4}$ is in somewhat remarkable agreement with the experimentally determined value of $\sim 10^{-4}$.

9. Summary

An extensive set of data that provides important new information about the HCN laser has been obtained by millimeter/submillimeter rotational absorption spectroscopic techniques. These experimental results have made possible the construction of a simple model which makes detailed and quantitative predictions that are in good agreement with both the new results and a large majority of the results previously reported in the literature. In this model the extremely non-thermal population of HCN(100) is attributed to near resonant vibrational transfer from electron impact excited $N_2(v=1)$. The population of HCN(100) is then efficiently transferred to the upper laser state HCN(110) by means of the rapid thermalization of the 1n0 bending stack. The rapid exchange of one unit of the bending quantum number for R/T energy also helps to maintain a large lasing inversion by relaxing the 0n0 bending stack and hence funneling excess population out of the lower laser state HCN(040). It should be emphasized that the very non-thermal population of HCN(100) is not due to the radiative metastability of this state [in fact HCN(100) appears to have a faster decay rate than HCN(001) because of the decay channel through the Coriolis perturbed level of

HCN(110)], but rather is due to the large concentration of vibrationally excited N_2 and the rapidity of the above near resonant vibrational exchange process.

The combination of this model and our experimental data accounts for:

1) The threshold current for laser oscillation and the dependence of the output power on the discharge wall temperature (Sect. 7).

2) The equilibrium between the CO($v=1$) and HCN(100) populations [CO($v=1$) would also contribute to the HCN(100) via near resonant vibrational transfer] and the changes in the vibrational state populations of HCN when CO is used as an admixture (Sect. 8.2).

3) The apparent major discrepancy between upper state lifetimes derived from Q-switching experiments previously reported in the literature (Sect. 8.1).

4) The observed laser induced competition effect on the population of HCN (100) and the absence of bottlenecks in the 0n0 bending stack (Sect. 5).

5) The overall efficiency of cw HCN discharge lasers (Sect. 8.4).

An unambiguous experimental check of the proposed vibrational transfer excitation mechanism could be performed by flowing discharge excited N_2 into pure HCN (with the mixing occurring in a discharge free region) in a continuous flow system similar to that described by Patel [38] for CO_2 and N_2. Depending on the flow and vibrational transfer rates, this sort of configuration may have potential for an increase in laser power since the partial pressure of HCN could be significantly larger than the small concentration that exists in discharge plasmas owing to the previously discussed electron impact dissociation (Sect. 6). However, it would entail the considerable inconvenience of flowing large quantities of HCN. The circumvention of the dissociation problem provided by this technique might also allow discharge driven far-infrared lasing with other polyatomic molecules.

Acknowledgements. The authors would like to thank Professor E. Herbst for many enlightening discussions and Professors B. Guenther and D. Robinson for graciously providing comments and criticisms of an initial draft of this paper. They would also like to thank the Research Corporation for support of the initial phases of this research.

References

1. H.A. Gebbie, N.W.B. Stone, F.D. Findlay: Nature **202**, 685 (1964)
2. D.R. Lide, Jr., A.G. Maki: Appl. Phys. Lett. **11**, 62–64 (1967)
3. L.O. Hocker, A. Javan, D. Ramachandra Rao, L. Frenkel, T. Sullivan: Appl. Phys. Lett. **10**, 147–149 (1967)
4. L.O. Hocker, A. Javan: Phys. Lett. **25A**, 489–490 (1967)
5. F.K. Kneubühl, C. Sturzenegger: In *Infrared and Millimeter Waves*, **3**, 219–274 (Academic Press, New York 1980)
6. J.P. Pichamuthu: In *Infrared and Millimeter Waves* **7**, 165–244 (Academic Press, New York 1983)
7. G.W. Chantry: *Submillimetre Spectroscopy* (Academic Press, New York 1971)
8. A.G. Maki, W.B. Olson, R.L. Sams: J. Mol. Spectrosc. **36**, 433–447 (1970)
9. W.W. Clark, F.C. De Lucia: J. Chem. Phys. **74**, 3139–3147 (1981)
10. W. Gordy, R.L. Cook: *Microwave Molecular Spectra* (Wiley, New York 1970)
11. C.H. Townes, A.L. Schawlow: *Microwave Spectroscopy* (McGraw-Hill, New York 1955)
12. F.C. De Lucia, P.A. Helminger: J. Chem. Phys. **67**, 4262–4267 (1977)
13. F.C. De Lucia: In *Molecular Spectroscopy, Modern Research*, Vol. 2, ed. by K. Narahari Rao (Academic Press, New York 1976) pp. 69–92
14. J.A. McGarvey, Jr., N.E. Friedman, T.A. Cool: J. Chem. Phys. **66**, 3189–3196 (1977)
15. H.J. Schötzau, F.K. Kneubühl: IEEE J. QE-**11**, 817–821 (1975)
16. F.C. De Lucia: Appl. Phys. Lett. **31**, 606–608 (1977)
17. D.W. Robinson: Opt. Commun. **27**, 281–286 (1978)
18. A.G. Maki, L.R. Blaine: J. Mol. Spectrosc. **12**, 45–68 (1964)
19. A. Yariv: *Quantum Electronics*, 2nd ed. (Wiley, New York 1975)
20. P. Belland, D. Veron: Opt. Commun. **9**, 146–148 (1973)
21. H.J. Schötzau, F. Kneubühl: Appl. Phys. **6**, 25–30 (1975)
22. C.K. Rhodes, A. Szöke: In *Laser Handbook*, Vol. 1, ed. by F.T. Arecchi, E.O. Shulz-Dubois (North-Holland, Amsterdam 1972) pp. 265–324
23. S. Kunstreich, J.P. Lesieur: Opt. Commun. **13**, 17–20 (1975)
24. G.A. West: Cyanide radical molecular electronic and vibrational chemical lasers; hydrogen cyanide polyatomic chemical lasers, Thesis, University of Wisconsin-Madison (1975)
25. M. Yamanaka, T. Yamauchi, H. Yoshinaga: Jpn. J. Appl. Phys. **10**, 1601–1603 (1971)
26. G. Jones, C.C. Bradley, J. Chamberlain, H.A. Gebbie, N.W.B. Stone, H. Sixsmith: Appl. Opt. **8**, 701–705 (1969)
27. P.G. Frayne: J. Phys. B **2**, 247–259 (1969)
28. W.M. Müller, G.T. Flesher: Appl. Phys. Lett. **10**, 93–94 (1967)
29. O.M. Stafsudd, F.A. Haak, K. Radisavljevic: IEEE J. QE-**3**, 618–620 (1967)
30. S.F. Dyubko, A.N. Topkov: Sov. J. Quantum Electron. **3**, 56–57 (1973)
31. B.E. Cherrington: *Gaseous Electronics and Gas Lasers* (Pergamon Press, New York 1979)
32. G.J. Schulz: Phys. Rev. **135**, A988–A994 (1964)
33. C.B. Moore, R.E. Wood, B. Hu, T.J. Yardley: J. Chem. Phys. **46**, 4222–4231 (1967)
34. C.B. Moore: *Fluorescence* (Dekker, New York 1967)
35. L.Y. Nelson, A.W. Saunders, Jr., A.B. Harvey: J. Chem. Phys. **55**, 5127–5128 (1971)
36. J.M. Flournoy, L.Y. Nelson: Chem. Phys. Lett. **6**, 521–524 (1970)
37. F.C. De Lucia, E. Herbst, M.S. Feld, W. Happer: IEEE J. QE-**17**, 2171–2187 (1981)
38. C.K.N. Patel: In *Lasers*, **2**, 1–190 (Dekker, New York 1968) 1968)
39. R.G. Gordon: J. Chem. Phys. **44**, 3083–3089 (1966)
40. D.D. Bicanic, A. Dymanus: Infrared Phys. **16**, 601–604 (1976)
41. J. Vanderkooy, C.S. Kang: Infrared Phys. **16**, 627–637 (1976)